Macromolecules

pubs.acs.org/Macromolecules
Article

Temperature and Pressure Effects on the Dynamics of Elastomeric Dioxaborolane Vitrimers

Michail Danikas, Matteo Conti, Johan Mattsson, Nathan J. Van Zee,* Renaud Nicolaÿ,* Laurence Ramos, and George Floudas*

Cite This: *Macromolecules* 2026, 59, 10544−10556

ABSTRACT: We report the synthesis, and the thermal, viscoelastic and dynamic properties of a series of dioxaborolane-based poly(*n*-butyl methacrylate) (PBMA) vitrimers, as a function of molar mass and cross-linking density. By combining calorimetry, dielectric spectroscopy and rheology, we explored the different characteristic temperatures that influence the dynamics of vitrimers. Three main processes could be identified by dielectric spectroscopy, the local β-process, the segmental α-process and the merged αβ-process at higher temperatures. Pressure was employed to examine their sensitivity through an apparent activation volume. We found that the local β-process was only weakly affected by pressure, and that the rubber-to-glass temperature continuously increased with vitrimer cross-linking density. Our results revealed that the dynamic bonds in vitrimers contribute to an effective unit of relaxation (e.g. an effective segment) that is larger than that in the corresponding homopolymer. In addition, the ratio of activation energies at constant volume and at constant pressure revealed that the segmental dynamics in the vitrimers is controlled by intra-molecular barriers. The viscoelastic properties are influenced by the topology freezing temperature, T_V, separating segmental-controlled dynamics at lower temperatures from the bond exchange mechanism at higher temperatures initiating the flow. The derivative approach applied to the viscoelastic shift factors was found to be a practical method to locate T_V. In the vitrimers, the bond exchange mechanism had a high apparent activation energy ($E \sim 90$ kJ/mol) similar to that of the segmental dynamics. We present the first high-pressure investigation of the relaxation dynamics in vitrimers, elucidating the origin of the segmental process and re-defining the fundamental effective unit of relaxation.

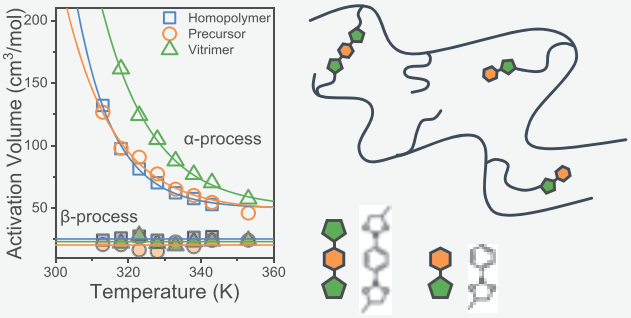

1. INTRODUCTION

Vitrimers are chemically cross-linked polymers that can flow at elevated temperatures.[1,2] They consist of a polymer network that can change its topology through degenerate exchange reactions without modifying its connectivity.[3−5] These dynamic networks can be reprocessed, thus exhibiting recyclability[1,6,7] as well as other unique properties, including shape memory[8,9] and self-healing ability.[10−12] A number of chemistries have been used to design vitrimers, including dioxaborolane metathesis.[3,13,14] In dioxaborolane metathesis, molecules reversibly exchange fragments linked together by the strong B−O bonds of the boronic ester groups, without the need for a catalyst. The chemical compatibility of dioxaborolanes with a large variety of chemical functions and species, as well as their high thermal stability, makes them ideal candidates to design vitrimers of various natures and topologies.[14,15] Dioxaborolane-based vitrimers can be synthesized by polymerizing functional monomers, for example, by radical polymerization,[3,13,14] or by chemical modification of commercial polymers, either in solution[13,16] or in bulk by reactive processing.[13,17−19]

Because of their recyclability, the viscoelastic properties of vitrimers have attracted considerable attention.[20−36] The viscoelastic properties of amorphous vitrimers are characterized by two temperatures. One temperature is the usual rubber-to-glass temperature, T_g, associated with the freezing of the segmental dynamics. The other temperature is the so-called topology freezing temperature, T_V, which is higher than T_g (the case $T_V < T_g$ is not considered here as this definition is not physically meaningful). At intermediate temperatures, $T_g < T < T_V$, the polymer behaves as an elastomer, and only at $T > T_V$, the exchange reactions speedup and the material transitions from an elastomer to a viscoelastic liquid. In the

Received: May 15, 2026
Revised: July 3, 2026
Accepted: August 17, 2026
Published: September 5, 2026

https://doi.org/10.1021/acs.macromol.6c01360
Macromolecules 2026, 59, 10544−10556

latter state, the flow is controlled largely—but not only—by the cross-link exchange kinetics.[16] Despite a good knowledge of the viscoelastic[20−36] and thermodynamic[37,38] changes around T_V, but the exact location of T_V is also debated as it requires a close inspection of the viscoelastic shift factors.

The current literature deals with the way the segmental dynamics influence the bond exchange dynamics. Different models have been proposed to account for their possible relation. A first model[22] naturally considered sequential dynamics, as proposed earlier for the self-healing process in polymer networks with reversible associating stickers.[39,40] According to this model, the time scale of bond exchange is $\tau_{exch.} = \tau\alpha\exp(E/RT)$, where $\tau\alpha$ is the relaxation time of the segmental process, and E is the apparent activation energy for the bond-breaking process. Other models[28,29] considered that the mechanism for the bond exchange time scale combines a diffusion-controlled activated process of cross-linking with an additional Arrhenius process that describes the bond exchange kinetics. Overall, the relevant quantity to differentiate between the different models is the ratio $\tau_{exch.}/\tau\alpha$, and its temperature dependence. In all the above, the definition of a "segment" is ill-defined. Invariably, theories consider the same segment as in the respective homopolymers.

Herein, a series of dioxaborolane-based poly(*n*-butyl methacrylate) (PBMA) vitrimers were synthesized. We report the thermal, viscoelastic, and dynamic properties of the vitrimers as a function of the molar mass of the functional thermoplastic precursor and the cross-link density of the network. Our aim is to address the following questions: What is the origin of the segmental dynamics in PBMA vitrimers? In particular, what is the fundamental effective unit of relaxation (the effective segment) in the vitrimers in comparison to the homopolymer? How can the topology freezing temperature, i.e., the temperature where the dynamics change from segmental mode dominated to bond exchange dominated, be located? Lastly, the apparent activation energy for the bond exchange mechanism is discussed in relation to the corresponding energy for the segmental process. Addressing some of the questions requires the use of pressure as an additional thermodynamic parameter in dielectric spectroscopy. It provides access to parameters such as the apparent activation volume, the pressure coefficient of T_g, and the ratio of activation energies at constant volume and constant pressure. These parameters were employed here, for the first time, to elucidate the origin of the segmental process in vitrimers together with the thermodynamic and viscoelastic properties.

2. EXPERIMENTAL SECTION

2.1. Synthesis

PBMA homopolymers and vitrimer precursors with number-average molar masses (M_n) ranging from 16 to 63 kg/mol and relatively low dispersities ($Đ \leq 1.3$) were prepared via reversible addition-fragmentation chain-transfer (RAFT) radical polymerization.[41] The functional monomer, 5,6-dihydroxyhexyl methacrylate (**DM**), and the cross-linker, 1,4-bis(4-methyl-1,3,2-dioxaborolan-2-yl)benzene (**CL**), were synthesized according to protocols reported in the literature.[13] The PBMA homopolymers (**H85** and **H290**) and the diol-functionalized PBMA copolymers (**D85**, **D306**, and **D348**) were synthesized through a one-pot reaction sequence consisting of RAFT (co)polymerization, aminolysis and Michael addition (Figure 1).[42] The two PBMA homopolymers had M_n values of 16 and 48 kg/mol (Table S1, Supporting Information). The functionalized copolymers **D85**, **D306**, and **D348**, which contained 9.2–12.0 mol % of **DM** based on ^{1}H NMR characterization, were converted into dioxaborolane vitrimer precursors through the condensation of the diol functional groups of **DM** with phenylboronic acid (Figure 1). Well-defined vitrimer precursors (**P85**, **P306** and **P348**) with M_n values of 22, 53 and 63 kg/mol were obtained (Table S2, Supporting Information). Following purification by reprecipitation, all precursors contained 9.2–10.4 mol % of units with pendant dioxaborolane groups, according to ^{1}H NMR spectroscopy. **P85**, **P306**, and **P348** were cross-linked in solution with various amounts of **CL** to produce the dioxaborolane-based vitrimers **V85-3%**, **V306-1%**, **V348-5%**, and **V348-9%**, after removal of the solvent and mono-dioxaborolane by-product under vacuum at 120 °C (Figure 1). **V85-3%**, **V306-1%**, **V348-5%**, and **V348-9%** presented a cross-linking density of 3, 1, 5 and 9 mol %, respectively (Table 1). The cross-linking density is defined as the molar ratio of cross-linked **DM** repeating units to the total number of repeating units. Details on the chemical structures, the NMR spectroscopy, SEC, and UV-Vis spectra are shown in Figures S2–S12, Supporting Information.

2.2. Differential Scanning Calorimetry (DSC)

Temperature-modulated (TM)-DSC measurements were performed using a Q2000 calorimeter (TA Instruments). A low-frequency sinusoidal signal was applied to the standard DSC profile, expressed as $T = T_0 + rt + A_T \sin(\omega t)$, where r is the heating rate, A_T is the modulation amplitude (±1.0 K), and ω is the angular frequency. The period/rate pairs used were as follows: 20 s/10.0, 40 s/5.0, 60 s/3.3, 100 s/2.0, and 150 s/1.3 K · min^{-1}. The temperature range for the TM-DSC measurements was 253 to 373 K. TM-DSC traces, along with their corresponding derivatives, are shown in Figure 2 for the high-molar-mass samples. Additional TM-DSC traces for the low-molar-mass samples are shown in Figure S13 and Figure S14. The traces display the reversing heat capacity as a function of temperature, which is used to extract the rubber-to-glass temperature (T_g) for the PBMA homopolymers, vitrimer precursors, and vitrimer samples.

2.3. Thermogravimetric Analysis (TGA)

The sample mass as a function of temperature was investigated with a Mettler Toledo TGA. Measurements were made in a N_2 atmosphere for a temperature range from 303 to 773 K with a heating rate of 10 K·min^{-1}. The results for vitrimers **V85-3%**, **V306-1%**, and **V348-5%** are shown in Figure S15. **V306-1%** was thermally stable below 533 K. **V348-5%** had a 2.3% mass loss below 533 K, whereas the lower-molar-mass vitrimer **V85-3%** exhibited a mass loss of 3.8% below 500 K.

2.4. Rheology

The viscoelastic properties of the samples were measured with an AR-G2 rheometer (TA Instruments), with a magnetic bearing that allowed low (nano-torque) control. Measurements at different temperatures were made with an environmental test chamber and a parallel plate geometry of 8 mm in diameter. The linear and nonlinear viscoelastic regimes were identified by recording the strain amplitude dependence of the complex shear modulus $|G^*|$, at frequency $\omega = 10$ rad · s^{-1}. Isothermal frequency scans were used to record the storage (G') and loss (G'') moduli in the frequency range from 0.1 to 100 rad · s^{-1} and for several temperatures. The time-temperature superposition (TTS) principle allows the frequency dependence of the complex modulus at any temperature to be determined from a master curve with a reference temperature, T_{ref}, as: $|G^*|(\omega, T) = b_T G^*(a_T\omega, T_{ref})$ where a_T and b_T are respective frequency-scale and modulus-scale shift factors. The shift factors, a_T can be described by the Williams–Landel–Ferry (WLF) equation:

$$\log(a_T) = \frac{-c_1^r(T-T_{ref})}{c_2^r + (T-T_{ref})} \quad (1)$$

https://doi.org/10.1021/acs.macromol.6c01360
Macromolecules 2026, 59, 10544−10556

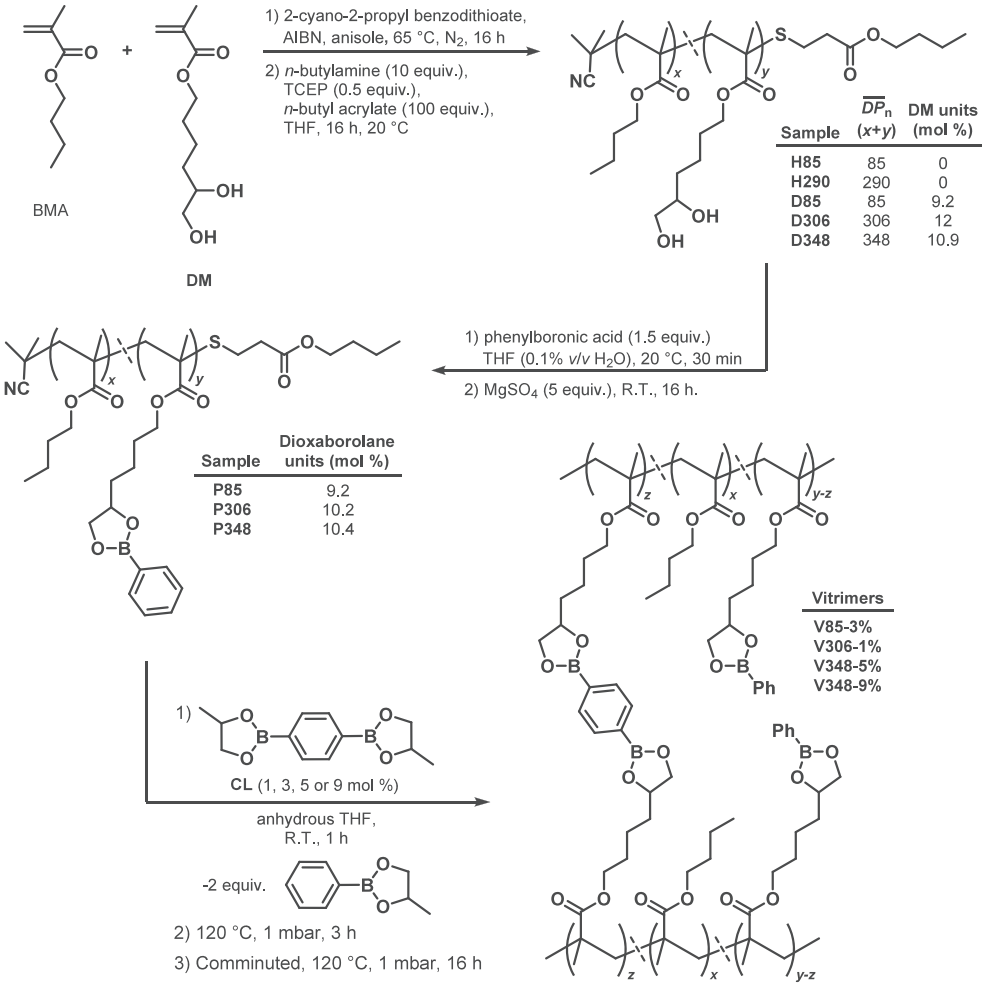

Figure 1. Synthesis of PBMA homopolymers and copolymers, vitrimer precursors, and dioxaborolane-based vitrimers. The average degree of polymerization ($\overline{DP}_n$) and the composition of the (co)polymers were determined by ^{1}H NMR spectroscopy, as described in the Supporting Information.

Table 1. List of Poly(n-butyl methacrylate) (PBMA) Vitrimer Samples with their Number-Average Molar Masses, *Đ*, Pendant Group and Cross-linking in *mol* %

sample	$\overline{DP}_{n,theo.}$ of precursor[a]	$M_{n,theo.}$ (kg/mol) of precursor[a]	M_n (kg/mol) of precursor[b]	*Đ* of precursor[b]	% dioxaborolane of precursor[c]	% cross-linking
V85-3%	85	13	22	1.2	9.2	3
V306-1%	306	48	53	1.2	10.2	1
V348-5%	348	55	63	1.2	10.4	5
V348-9%	348	55	63	1.2	10.4	9

[a]Calculated from RAFT equation for $\overline{DP}_n$ and for $\bar{M}_{n,\,theo}$. [b]Determined by size exclusion chromatography. [c]Determined by ^{1}H NMR spectroscopy.

where T is the temperature, T_{ref} is the reference temperature used to construct the master curve. c_1^r and c_2^r are empirical constants, obtained at the reference temperature. Once the rubber-to-glass temperature is determined, the corresponding parameters for the glassy region, c_1^g and c_2^g can be calculated as follows:

$$c_1^g = \frac{c_1^r c_2^r}{c_2^r + (T_g - T_{ref})}, \quad c_2^g = c_2^r + T_g - T_{ref} \tag{2}$$

2.5. Dielectric Spectroscopy (DS)

DS measurements were performed with a Novocontrol BDS system with a frequency response analyzer (Novocontrol Alpha) for frequencies f in the range from 10^{-2} to 3×10^6 Hz. The isobaric measurements were carried out at ambient pressure (0.1 MPa) over a temperature range from 393 to 203 K, in 5 K increments. Samples were stabilized at each temperature (within 0.05 K) for at least 20 min to achieve thermal equilibrium. DS measurements were made in the parallel plate electrode geometry. For the homopolymers and vitrimer precursors,

https://doi.org/10.1021/acs.macromol.6c01360
Macromolecules 2026, 59, 10544−10556

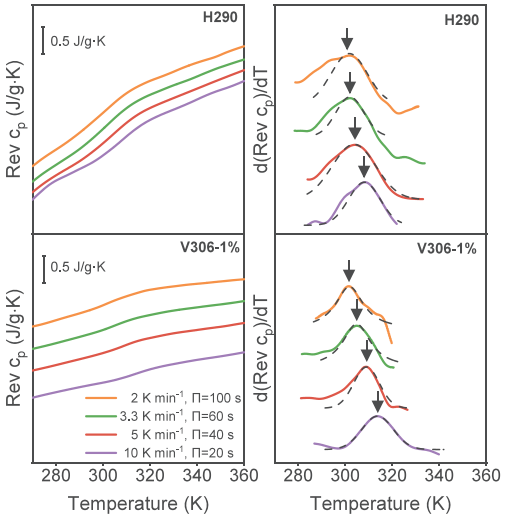

Figure 2. Temperature dependence of reversing heat capacity for the high-molar-mass PBMA homopolymer **H290** (top left) and vitrimer **V306-1%** (bottom left), obtained from TM-DSC at different periods of modulation, $\Pi = 100$ *s*, 60 *s*, 40 *s*, and 20 *s*, as indicated, alongside with their derivative with respect to T (right). The arrows depict the T_g values also listed in Table S3.

we used electrodes of diameter 20 mm with a constant spacing maintained by poly(tetrafluoroethylene) (Teflon) spacers of thickness 50 μm. For vitrimers, the diameter of the electrode was 10 mm, and the thickness was around 150 μm. Measurements under hydrostatic pressure were carried out in a Novocontrol pressure cell. The pressure setup consisted of a *T*-controlled cell and hydraulic closing press with an air pump for hydrostatic test pressure. For the *P*-dependent measurements, the samples were placed between 20 mm electrodes, and Teflon spacers were used to maintain the thickness (typically 50 μm) for the homopolymers and vitrimer precursors. Subsequently, the capacitor was wrapped with Teflon tape and placed inside a Teflon ring in order to prevent the flow of silicone oil (Dow Corning 550 Fluid) into the sample. Silicone oil is the liquid that uniformly transmits pressure to the capacitor. The isothermal measurements were performed with temperature stability better than 0.2 K and pressure stability better than 2 MPa. Both in isothermal and isobaric measurements, the complex dielectric function, $\varepsilon^*(\omega, T, P) = \varepsilon'(\omega, T, P) - i\varepsilon''(\omega, T, P)$, where ε' is the real and ε'' is the imaginary part, was obtained as a function of frequency, ($f = \omega/2\pi$), temperature, T, and pressure, P.[43,44] At a given temperature and pressure, the complex dielectric function and the respective dielectric loss curves can be fitted by the empirical equation of Havriliak and Negami (HN):[43,44]

$$\varepsilon^*(\omega, T, P) = \varepsilon_\infty + \sum_k \frac{\Delta\varepsilon_k(T,P)}{\left[1 + \left(i\cdot\omega\cdot\tau_{HN,k}(T,P)\right)^{m_k}\right]^{n_k}} + \frac{\sigma_0(T,P)}{i\varepsilon_0\omega} \quad (3)$$

where $\Delta\varepsilon k$ is the dielectric strength, $\tau_{HN,\,k}$ is the HN characteristic relaxation time and the index k indicates the process under investigation. At lower frequencies, the dielectric loss sharply rises due to conductivity contributions as $\sigma_0/\varepsilon_0\omega$, where σ_0 is the dc-conductivity and ε_0 ($= 8.854 \times 10^{-12}$ F · m^{-1}) is the permittivity of free space. The parameters m_k and n_k ($0 < m_k, m_k n_k \leq 1$) are two shape parameters of the H–N function that describe the symmetric and asymmetric broadening of the distribution of relaxation times, respectively. The characteristic relaxation times at maximum loss ($\tau max = 1/2\pi f_{max}$, where f_{max} is the characteristic peak frequency of the dielectric loss) are presented herein and have been analytically obtained from the Havriliak–Negami equation as follows:

$$\tau_{max,k} = \tau_{HN,k}\left[\sin\left(\frac{\pi m_k n_k}{2(1+n_k)}\right)/\sin\left(\frac{\pi m_k}{2(1+n_k)}\right)\right]^{1/m_k} \quad (4)$$

In the analysis of the dynamic behavior, we have used the ε'' values at every temperature. Moreover, we employed the principle of the time–temperature superposition (tTs) in isobaric dielectric measurements, which allows the frequency dependence of the complex $\varepsilon^*(\omega)$ at any temperature to be determined from a measurement at a reference temperature from the "master curve." The shift factors, αT, were fitted according to the WLF equation.

3. RESULTS AND DISCUSSION

We first discuss the thermodynamics and the effect of vitrimer units on the rubber-to-glass temperature, T_g. We then present the results for the segmental dynamics as a function of temperature and pressure. Lastly, we discuss the viscoelastic properties. In particular, we are interested in locating the characteristic temperature T_V, and in investigating the relationship between the bond exchange mechanism and the segmental dynamics.

3.1. Thermodynamics

The TM-DSC traces allow extracting T_g from the peak position of the derivative of the reversing heat capacity (c_p), (see black arrows in Figure 2). To ensure efficient deconvolution of the modulated signal, the number of cycles was set to five, with a T_g breadth (ΔT_g) of about 20 *K*.

The values of T_g obtained from TM-DSC measurements for the PBMA homopolymers, vitrimer precursors, and vitrimer samples of different molar masses and cross-link densities are plotted in Figure 3, and in Figures S13 and S14. The values of T_g for different modulation periods are provided in Table S3. As expected, the higher molar mass homopolymer exhibits a higher T_g. Furthermore, T_g follows the expected trend: $T_g^H < T_g^P < T_g^V$, where superscripts H, P and V refer respectively to homopolymer, vitrimer precursor and vitrimer. The increase in T_g^V is very pronounced for the high molar mass vitrimer

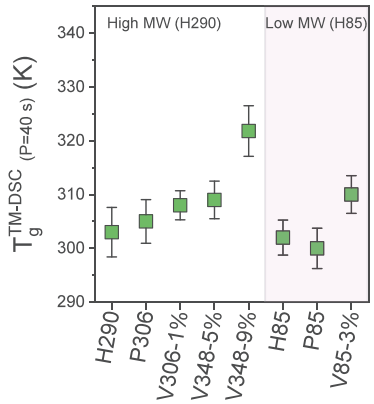

Figure 3. Liquid-to-glass temperatures for PBMA homopolymers and vitrimer precursors with different molar masses and the rubber-to-glass temperatures of the corresponding vitrimers with different cross-linking densities. Data were obtained from TM-DSC (modulation period of 40 s). The vertical lines indicate the FWHM of the $d(c_p)/dT$ peaks.

https://doi.org/10.1021/acs.macromol.6c01360
Macromolecules 2026, 59, 10544–10556

V348-9% (~ 20 K). This trend shows that the introduction of cross-links restricts backbone mobility and thus increases T_g.

3.2. Segmental and Local Dynamics Measured by Dielectric Spectroscopy

3.2.1. Role of Temperature. Insight into the temperature dependence of the molecular dynamics at the segmental and local levels can be obtained through dielectric spectroscopy measurements. Representative dielectric loss curves for the vitrimer **V348-5%** are presented in Figure 4 (top). In contrast to rheology (see below), DS time-temperature superposition breaks down in the vicinity of T_g. This is due to the presence of two dielectrically active processes with distinctly different temperature dependencies (α- and β-processes) that merge into a single αβ-process at higher temperatures.[45,46] The extracted characteristic frequencies at maximum loss, f_{max}, for the different processes are depicted in Figure 4 (bottom) for the vitrimer **V306-1%**. Starting from lower temperatures, the fast γ-process, associated with a local relaxation of the polar side group, is observed with an activation energy of 28 ± 2 kJ/mol. At higher temperatures two distinct processes exist: the α-process, which is associated with the segmental motion, and the β-process, which is often attributed to localized molecular motions in amorphous polymers. By increasing temperature, the two processes merge into a single αβ-process. This behavior is consistently observed across all PBMA samples, as shown in Figure S16.

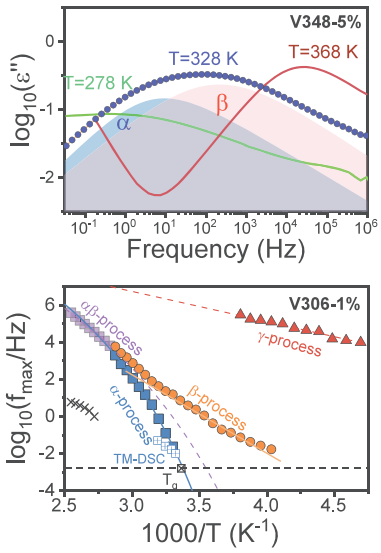

Figure 4. (Top) Representative dielectric loss curves for the PBMA vitrimer **V348-5%**. The three curves correspond to 278 K (green line), 328 K (blue spheres) and 368 K (red line). For the dielectric loss curve at 328 K the deconvolution into the α- (in light blue) and β- (in light red) processes is shown. (Bottom) Characteristic frequencies at maximum loss plotted as a function of inverse temperature for the vitrimer **V306-1%**. The purple squares indicate the αβ-process, the blue squares the α-process, the orange circles the β-process, and the red triangles the faster γ-process. The open squares with crosses depict the α-process from TM-DSC for the different modulation periods. The horizontal dashed line is the frequency used to extract the rubber-to-glass temperature (corresponding to $\tau = 100$ s). Additionally, a slower process is identified in DS at the crossings of ε', and ε'', corresponding to the motion of ions.

On the one hand, the characteristic frequencies at maximum loss for the αβ- and α-processes follow the Vogel-Fulcher-Tammann (VFT) temperature dependence:

$$f_{max} = f_\infty e^{-\frac{B}{T-T_0}} \quad (5)$$

Here, f_∞, is the limiting frequency at very high temperatures (typically ~ 10^{13} Hz consistent with lattice vibrations), B is the activation parameter, and T_0 is the "ideal" glass temperature located below the conventional T_g. On the other hand, the characteristic frequencies at maximum loss for the β- and γ-processes follow an Arrhenius law:

$$f_{max} = f_\infty e^{-\frac{E}{RT}} \quad (6)$$

with E the Arrhenius activation energy. Values of the fitting parameters for the VFT and Arrhenius laws , respectively, with standard errors from the fitting procedure are provided in Table 2 and Table S4, respectively. A summary of the VFT dependencies for the segmental process in the high-molar-mass PBMA samples, including all vitrimers, is depicted separately in Figure 5. We found a slower segmental process, and concomitantly, an increasing T_g with increasing cross-linking density. The corresponding plots for the merged αβ-process and the more local β-process are shown in Figure S17. In general, the dynamics associated with the αβ-process show similar trends as the one associated with the α-process; increasing cross-linking density slows down the dynamics. As for the β-process, an Arrhenius temperature dependence of the characteristic frequencies is evident only at lower temperatures (activation energies reported in Table S4 were extracted from this range). At higher temperatures, there are noticeable deviations from the Arrhenius temperature dependence for the β-process. Nevertheless, the effect of vitrimer formation on the β-process is minor, in sharp contrast to the αβ-process and more importantly to the α-process. In addition to the vitrimer effect on the dynamics, there is an appreciable effect on the broadening of the dielectric loss curves at all temperatures. This can be quantified by the values of the low-frequency shape parameter, m_k, that is a strong function of vitrimer content and temperature (Figures S18 and S19). It suggests that increasing cross-linking density creates a distribution of relaxation times reflecting the distribution of local environments.

Table 2. VFT Parameters for the Merged *αβ*-Process and the *α*-Process (Segmental) Obtained by DS for High- and Low-Molar-Mass PBMA

	αβ-process[a]		*α-process*[a]	
sample	B (K)	T_0 (K)	B (K)	T_0 (K)
homopolymer **H290**	3790 ± 40	177 ± 2	2990 ± 60	214 ± 2
precursor **P306**	3850 ± 30	173 ± 2	3070 ± 50	209 ± 2
vitrimer **V306-1%**	3730 ± 30	181 ± 1	3100 ± 50	212 ± 2
vitrimer **V348-5%**	3700 ± 30	186 ± 1	3050 ± 60	220 ± 2
vitrimer **V348-9%**	4002 ± 60	174 ± 3	2763 ± 70	235 ± 2
homopolymer **H85**	3840 ± 20	172 ± 1	3890 ± 140	183 ± 5
precursor **P85**	3850 ± 15	170 ± 1	3290 ± 60	200 ± 2
vitrimer **V85-3%**	3720 ± 40	181 ± 2	3100 ± 50	212 ± 12

[a]Log(f_∞/Hz) is kept constant at 13.2 throughout the fitting procedure (to typical vibrational frequencies).

https://doi.org/10.1021/acs.macromol.6c01360
Macromolecules 2026, 59, 10544−10556

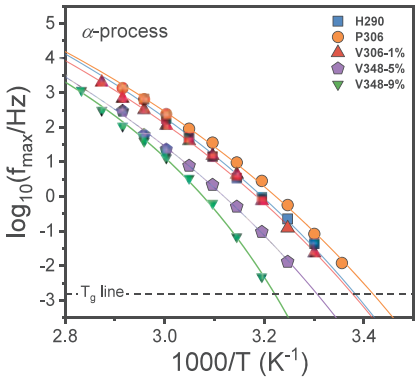

Figure 5. Characteristic frequencies at maximum loss of the α-process versus inverse temperature for the high-molar mass PBMA samples. The full-colored lines are best fits according to the VFT equation (eq 5). The horizontal dashed line indicates the frequency corresponding to $\tau = 100\ s$ ($\tau = 1/2\pi f_{max}$), which is used to obtain the liquid-to-glass temperature for the thermoplastic polymers and the rubber-to-glass temperature for the vitrimers.

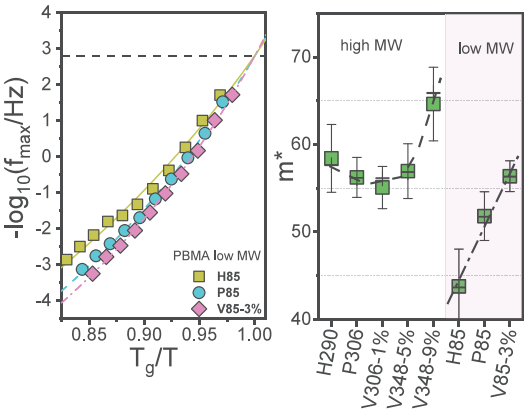

Figure 6. (left) Characteristic frequencies for the *a*-process as a function of T_g/T for the low-molar-mass homopolymer (**H85**), vitrimer precursor (**P85**), and vitrimer (**V85-3%**). (right) Calculated fragility for all samples (H: homopolymer, P: precursor, V: vitrimer). The black dashed lines are to guide the eye.

Another parameter characterizing the segmental process is the fragility or steepness index, m, defined as $\partial \log \tau/\partial(T_g/T)|_{T=T_g}$.[47] It quantifies the deviation of the temperature dependence of the relaxation times/frequencies from the Arrhenius behavior at $T \geq T_g$. It can be calculated using the VFT parameters as $m^* = \frac{BT_g}{2.303(T_g - T_o)^2}$. A higher (lower) value of fragility corresponds to a steeper (smoother) increase in the characteristic frequencies near T_g, indicating a more "fragile" ("strong") glass-forming system. The temperature dependence of the characteristic frequencies for the segmental process is shown in Figure 6 in a T_g-scaled plot together with the corresponding values of fragility. By comparing the lower and higher molar mass homopolymers we note an increasing steepness index with molar mass. This observation aligns with experimental results from various homopolymers[48] and with theoretical predictions.[49,50] In addition, an increase in fragility is observed (Figure 6) for the low-molar-mass vitrimer. This is typically associated with changes in chain stiffness. For the high-molar-mass samples, the vitrimers exhibit an increase in fragility with increasing cross-link density.

A key observation of the combined TM-DSC and DS results is the shift of the segmental process to lower frequencies and an increasing T_g, from homopolymer, to precursor, to vitrimer samples (Figure 5), indicating that the dynamic cross-links impose constraints on backbone mobility. Unexpectedly, the segmental relaxation time (α-process) of the vitrimer precursor was somewhat shorter with respect to the homopolymer. This could reflect the plasticizing role of the pendant dioxaborolane functionality. Compared with TM-DSC, the T_g values from DS are about 10 K lower, and they are within $\pm$ 2 K of the rheology measurements (see below, Figure 14). In addition, the temperature at which the α- and β-processes merge has the same dependence with the T_g, increasing with the cross-linking density of vitrimers (Figure 14). This is understandable as vitrimers slow down the segmental process but have a minor effect on the β-process. Apart from the increasing T_g, increasing cross-linking density increases the fragility especially for the low-molar-mass samples. This can be accounted for by the constraints of the α-process imposed by cross-links.

3.2.2. Role of Pressure. Quantitative insight into the molecular origin of the α-process can be obtained by pressure-dependent dielectric measurements.[44,45] Pressure is particularly important because it allows the separation of processes that are merged under ambient conditions. This reflects the different pressure sensitivity of the α- and β-processes. Furthermore, the apparent activation volume is a quantity closely linked to the molecular volume responsible for the process. Lastly, pressure-dependent studies offer valuable information on the molecular origin of the rubber-to-glass transition.

Here, we investigate the pressure sensitivity of the various relaxation processes and of the rubber-to-glass temperature T_g. To the best of our knowledge, this is the first time that the pressure dependence of the α- and β-processes is investigated in vitrimers. By applying pressure, the single αβ-process splits into the α-process and the β-process, implying that the former exhibits higher pressure sensitivity. This is indicated in Figure 7a for the high molecular weight vitrimer with 5% cross-links. At ambient pressure the dielectric loss curve corresponds to the merged αβ-process. We mention here that the merged αβ-process is a distinct process with characteristics closer to the α- than to the β-process.[45] Increasing pressure brings about the separation into two processes under isothermal conditions. The pressure dependence of the characteristic relaxation frequencies for the α-process (Figure 7b) follows the pressure equivalent of the VFT equation,[51]

$$f_{max} = f_\infty \exp\left(-\frac{D_P P}{P_0 - P}\right) \quad (7)$$

Here, f_∞ is the characteristic frequency at atmospheric pressure at a given temperature, D_P is a dimensionless parameter, and P_0 is the pressure corresponding to the "ideal" glass. The D_P value was held fixed to 11.6, a numerical value obtained by free fitting the data set with highest fidelity ($T = 333\ K$) for the α-process. Expectedly, the more local β-process exhibits a weaker pressure dependence (Figure 7b).

https://doi.org/10.1021/acs.macromol.6c01360
Macromolecules 2026, 59, 10544−10556

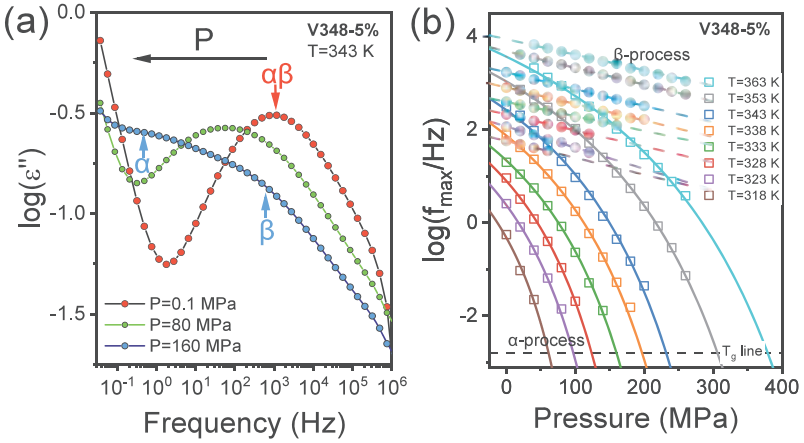

Figure 7. (a) Dielectric loss curves for the vitrimer **V348-5%** measured at a fixed temperature (343 K) and under different pressures as indicated, showing the effect of pressure on separating the α- and β-processes. (b) Characteristic frequencies at maximum loss plotted as a function of pressure, for the α-process (open squares) and the β-process (open circles). Different colors indicate different temperatures as indicated. Continuous lines are best fits with eq 7 and dotted lines are linear fits. The horizontal dashed line indicates the frequency corresponding to $\tau = 100\ s$ ($\tau = 1/2\pi f_{max}$), used to obtain the rubber-to-glass temperatures.

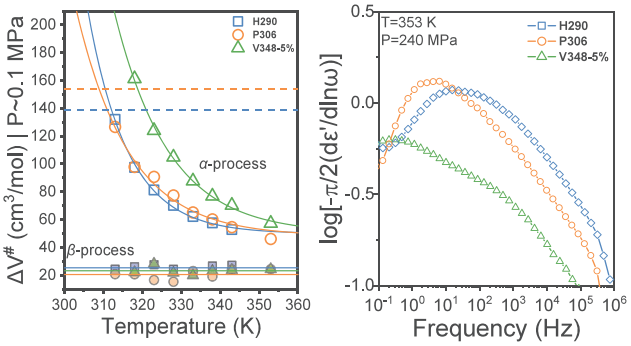

Figure 8. (left) Apparent activation volume ($\Delta V^{\#}$) as a function of temperature for the α-process (open symbols) and the β-process (filled symbols), for the high-molar-mass homopolymer **H290**, vitrimer precursor **P306**, and vitrimer **V348-5%.** The dashed lines indicate the molar volume of the repeat unit, V_{ru}, for the homopolymer and the precursor. The colored solid lines are guides for the eye. (right) Derivative of dielectric permittivity for the homopolymer **H290**, vitrimer precursor **P306**, and vitrimer **V348-5%**, at $T = 353$ K and $P = 240$ MPa, demonstrating the difference in the pressure sensitivity of the α-process for the three polymers.

The pressure sensitivity of the processes can be quantified by the apparent activation volume, $\Delta V^{\#}$, defined as,[44,45,52−55]

$$\Delta V = 2.303RT\left(\frac{\partial log\tau}{\partial P}\right)_T \tag{8}$$

The T-dependence of $\Delta V^{\#}$ at ambient pressure is depicted in Figure 8a. The apparent activation volume for the α-process exhibits a strong T-dependence approaching the molar volume of the repeat unit ($\Delta V_{r.u.}{}^{\#} \sim 140\ cm^3 \cdot mol^{-1}$) at about 15 K above T_g. This finding is consistent with earlier studies that associated the apparent activation volume with the molecular volume responsible for the motion at temperatures near T_g.[52−55] On the other hand, the β-process has a lower apparent activation volume ($\Delta V^{\#} \sim 25\ cm^3/mol$) that is independent of temperature.[55] The numerical value of $\Delta V^{\#}$ is a small fraction of the molar volume of the repeat unit (∼ 18%), suggesting the local origin of the β-process. We also observe that the apparent activation volume of the homopolymer is similar to that of the precursor, while the vitrimer shows stronger pressure sensitivity. The data demonstrate that the fundamental effective unit of relaxation responsible for the α-process in the case of vitrimers is significantly larger than that of homopolymer and vitrimer precursor. At the highest measurement temperature (353 K) with the least influence of T_g, the $\Delta V^{\#}$ of the vitrimer is about 20% higher than in the precursor polymer. Hence, dynamic covalent bonds effectively increase the size of the segment and slow down the α-process.

Additional information on the α-process can be obtained from the pressure coefficient of T_g, $d(T_g)/dP$. The value of T_g is obtained by extrapolating the VFT equation from the isothermal and isobaric plots (Figure 9). The extracted values of T_g exhibit qualitatively similar pressure dependence, which can be described by the following empirical equation[56]

$$T_g(P) = T_g(0)\left(1 + \frac{\nu}{\mu}P\right)^{1/\nu} \tag{9}$$

where $T_g(0)$ is the rubber-to-glass temperature at ambient pressure, and ν and μ are polymer specific parameters. The values are summarized in Table 3. For the homopolymer **H290**, the pressure coefficient $d(T_g)/dP\ |_{T_g} \sim 238 \pm 7$ K/GPa) which should be compared with the corresponding values for PMMA (240 K/GPa) and PEMA (234 K/GPa).[45] The pressure coefficient in the limit of ambient pressure increases from the homopolymer to the vitrimer precursor, and to the vitrimer. This again is consistent with the higher pressure sensitivity of the segmental process in the vitrimers.

Apart from the separation of molecular processes under isothermal conditions, pressure can provide additional information on the origin of the dynamic processes. For the liquid-to-glass transformation, theoretical predictions[44,57,58] consider two

https://doi.org/10.1021/acs.macromol.6c01360
Macromolecules 2026, 59, 10544−10556

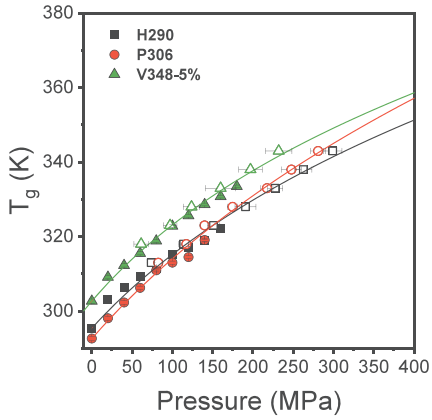

Figure 9. Pressure dependence of T_g for the homopolymer **H290**, vitrimer precursor **P306**, and vitrimer, **V348-5%**, as obtained at a characteristic time $\tau = 100$ *s*. The solid lines represent fits to the empirical equation (eq 9). Open and filled symbols are T_g values obtained from the "isothermal" and "isobaric" data, respectively.

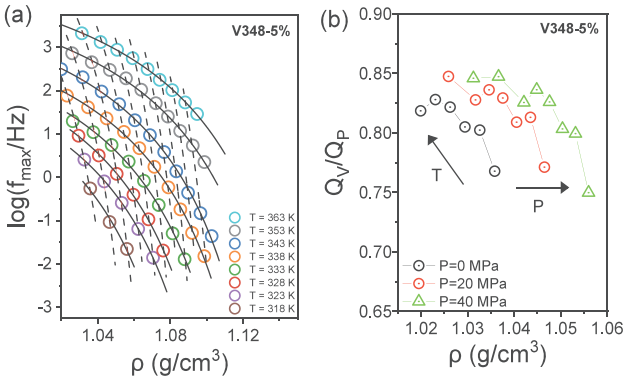

Figure 10. (a) Characteristic frequencies at maximum loss vs density for data obtained under *isothermal* (dashed lines) and *isobaric* (solid lines) conditions for the vitrimer **V348-5%**. The solid lines and dashed lines are the result of the fits to the modified VFT equation for the α-process. (b) Ratio $Q_V/Q_P = \Delta E^{\#}/\Delta H^{\#}$, of the constant-volume activation energy ($\Delta E^{\#}$) to the enthalpy of activation ($\Delta H^{\#}$) for the α-process plotted against density. Arrows indicate increasing temperature and pressure.

Table 3. Parameters of the Empirical Equation for the Pressure Dependence of T_g

polymer	μ (*MPa*)	ν	$T_g(0)$ (*K*)[a]	$d(T_g)/dP\|_{T_g}$ (*K*/*GPa*)
homopolymer, **H290**	1235 ± 85	7 ± 1	295	238 ± 7
precursor, **P306**	1179 ± 64	5 ± 1	293	247 ± 5
vitrimer, **V348-5%**	1193 ± 69	7 ± 1	303	253 ± 3

[a]Value held fixed to the $P = 0.1$ MPa value.

extreme cases: (a) free-volume theories, and (b) thermally activated processes on a constant-density "energy landscape." Since changing temperature affects both the thermal energy and the volume, *V*, it is impossible to separate the two effects by varying temperature alone. In order to disentangle the effects of *T* and *V* on the dynamics, pressure-dependent measurements are of paramount importance, since pressure can be applied isothermally (affecting only *V*). It has been proposed many years ago[57,58] that the ratio, $\Re$, of the apparent activation energy at constant volume, $Q_V = R(\partial[\ln\tau]/\partial(1/T))_V$, to that at constant pressure, $Q_P = R(\partial[\ln\tau]/\partial(1/T))_P$, provides a quantitative measure of the relative contributions of *T* and *V* on the segmental dynamics. Values of $\Re$ theoretically span the range 0 to 1. Values near unity suggest that the segmental dynamics are governed mainly by thermal energy (i.e., by intra-molecular energy barriers), whereas values near zero suggest the importance of intermolecular interactions through the available or "free" volume (in this case $Q_V = 0$). Earlier studies[55] explored the correlation between the repeat unit volume and the dynamic quantity $\Re$. It was shown that repeat unit volume and local packing play a key role in controlling the value of this ratio and thus the dynamic arrest at the liquid-to-glass temperature.

The ratio $\Re = Q_V/Q_P$ is also the ratio of the constant-volume activation energy ($\Delta E^{\#}$) to the enthalpy of activation ($\Delta H^{\#}$), $\Re = Q_V/Q_P = \Delta E/\Delta H$. Experimentally, it can be obtained by "coupling" the characteristic frequencies at maximum loss obtained under *isothermal* and *isobaric* conditions with the density through the equation of state. For the latter we employ the Tait equation,[59] $V(T, P) = V(T,0)[1 - 0.0894 \ln(1 + P/B(T))]$, where the temperature dependence of volume at fixed pressure is described by a quadratic function, $V(T,0) = V_0 + V_1T + V_2T^2$, and $B(T) = b_0 \exp(-b_1T)$. We have assumed the same parameters for the equation of state for the vitrimer as for the homopolymer. This procedure expresses the characteristic frequencies of the segmental process as a function of density (Figure 10a). The data can be fitted by the density-modified VFT equation,[44,52−55]

$$f_{max} = f_0 \exp\left(-\frac{D_\rho \rho}{\rho_0 - \rho}\right) \quad (10)$$

where $D\rho$ (isothermal, $D\rho T$, and isobaric, $D\rho P$) is a dimensionless parameter and ρ_0 is the density at the ideal glass temperature (T_0). Then the ratio, Q_V/Q_P, for the vitrimer **V348-5%** can be obtained directly at the crossings of the "isotherms" and "isobars" (Figure 10a). The *P*- and *T*-dependence of the ratio Q_V/Q_P is depicted in Figure 10b. For all investigated (T, P) conditions Q_V/Q_P is in the range ~0.75–0.85. Comparable values, close to 1, are measured for homopolymers, precursors and vitrimers (see additional data in Figure S20). These results indicate in particular that temperature and the associated intramolecular barriers are the main controlling parameters of the segmental dynamics in vitrimers.

3.3. Viscoelastic Properties

Here we report the linear viscoelastic properties of PBMA vitrimers, in comparison to the corresponding homopolymers and vitrimer precursors. Frequency sweep experiments were conducted over a range of temperatures, and the resulting data can be discussed either directly from the van Gurp-Palmen (vGP) plots or by attempting to construct master curves via time-temperature superposition (TTS). We first discuss the viscoelastic properties based on the vGP plots.[60] This approach bypasses the need for data shifting or time-temperature superposition, providing a more straightforward assessment of the

https://doi.org/10.1021/acs.macromol.6c01360
Macromolecules 2026, 59, 10544−10556

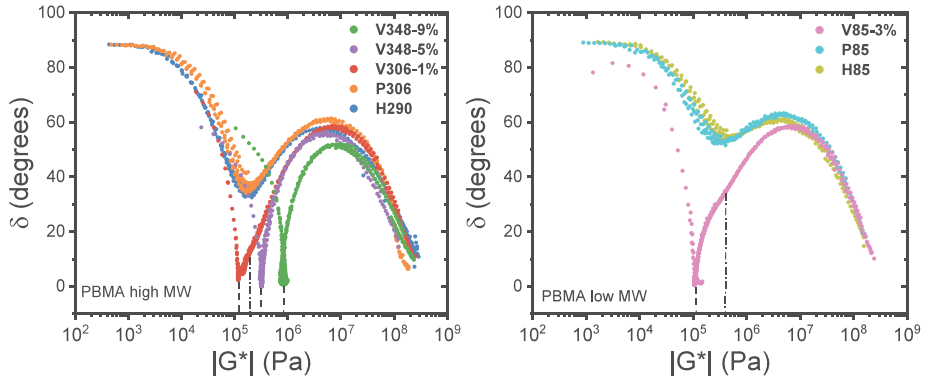

Figure 11. The van Gurp–Palmen (vGP) plot for (left) the high-molar-mass homopolymer **H290**, vitrimer precursor **P306**, and vitrimers with 1% (**V306-1%**), 5% (**V348-5%**), and 9% (**V348-9%**) cross-links, and (right) the low-molar-mass homopolymer **H85**, vitrimer precursor **P85**, and vitrimer with 3% cross-links (**V85-3%**). The rubbery plateau modulus can be identified (vertical dashed lines).

Table 4. Parameters Extracted from the vGP Plots (Figure 11) at Varying Cross-link Densities and Molar Masses

sample	$M_{n,theo.}(kg \cdot mol^{-1})^a$	$DP_{n,theo}$	δ_{min} (°)	G_N^0 ($\times 10^5 Pa$)	C (%)[b]	CN_f[c]	$M_{xx,theo}$(kg/mol)[d]	N_{xx}[e]
H290	41	290	32	1.8				
P306	48	306	34	1.6				
V306-1%	48	306	2.27	1.1	1	3.1	11.7	75
V348-5%	55	348	0.12	3.2	5	17.4	3.0	19
V348-9%	55	348	0.7	8.3	9	31.3	1.7	11
H85	12	85	53	3.9				
P85	13	85	52	3.3				
V85-3%	13	85	0.46	1.1	3	2.6	3.63.6	23

[a]Calculated from RAFT equation (see Supporting Information section). [b]Cross-links per total number of repeat units in mol %. [c]Average number of crosslinks per chain. [d]Theoretical molar mass between crosslinks ($M_{xx,theo} = M_{n,theo}/(CN_f+1)$). [e]Theoretical number of repeat units between cross-links.

material's inherent response. Figure 11 depicts the vGP results for the high- (left) and low-molar-mass (right) samples. Starting from the terminal regime ($\delta = 90^\circ$, low $|G^*|$) and moving across the modulus scale, δ decreases and reaches a minimum at δ_{min}, corresponding to the plateau modulus (G_N^0). Generally, the more entangled the polymer, the deeper the minimum is. As $|G^*|$ increases, δ increases and reaches a maximum before decreasing towards the "glass transition" (typically $|G^*| \approx 10^9 Pa$). For the homopolymer and precursor polymer, the plateau is not well-defined, resulting in a shallow minimum. For vitrimers, by contrast, the minimum in δ is very steep, and a systematic increase of the modulus at δ_{min} is observed with increasing cross-linker density. The numerical values for δ_{min} and G_N^0 values are given in Table 4 for all samples investigated. In addition, Table 4 provides some structural characteristics for both the high- and low-molar-mass samples, including the molar mass between cross-links, M_{xx}, and the respective number of repeat units N_{xx}. Note that the latter values are significantly smaller than the entanglement molar mass of PBMA (corresponding $N_e \sim 125$).

For the high-molar-mass vitrimer **V306-1%**, there is a shoulder (Figure 11, dashed-dot line) near δmin. Its value is in the proximity of the homopolymer (**H290**) and the precursor (**P306**) plateau values. The shoulder is also observed for the low-molar-mass sample. Overall, the shoulder in the **V306-1%** and **V85-3%** vitrimers may suggest an inhomogeneous distribution of cross-links.

The second approach to analyze the viscoelastic data uses master curves for the storage (G') and loss (G'') moduli. The procedure is as follows. First, we choose a reference temperature within the segmental-dominated dynamics (T_{ref} = 353 K) and then shift the data first horizontally in the loss tangent and subsequently vertically, in order to reach the best overlap of the data measured at different temperatures. The resulting master curves obtained for high- and low-molar-mass PBMA are shown, respectively, in Figures 12 and 13. These curves exhibit deviations from perfect time-temperature superposition (TTS), especially in the temperature region corresponding to the plateau, demonstrating thermorheological complexity.[24,32,36] A linear viscoelastic study[36] of poly(*n*-butyl acrylate) (PBA) vitrimers attributed the failure of TTS to two features: (i) the different temperature dependencies of the segmental dynamics and of the exchange dynamics of the cross-links, and (ii) the complex dynamics of the cross-linking points that are loosely connected to the network.

The linear viscoelastic response of the vitrimers exhibits a different response compared to the homopolymer and precursor samples. Vitrimers show a terminal region (flow) at high temperatures, an elastic plateau regime corresponding to the network-like behavior, an intermediate region and a transition into the glassy state (e.g., the segmental process). Some key relaxation frequencies are shown, which are associated with the terminal relaxation, the onset of entanglements, and the liquid-to-rubber transition (denoted by crossed circles). To

https://doi.org/10.1021/acs.macromol.6c01360
Macromolecules 2026, 59, 10544−10556

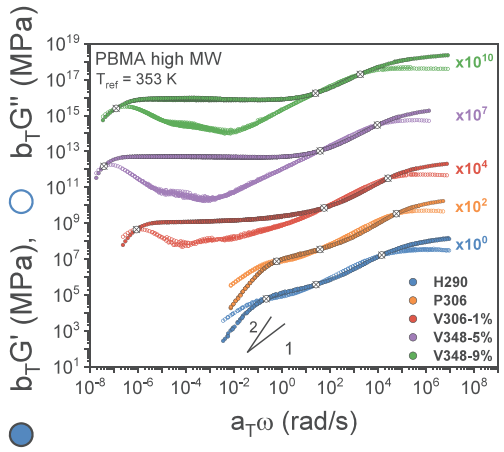

Figure 12. Master curves of the storage (G'-filled symbols) and loss (G''-open symbols) moduli of PBMA homopolymer (**H290**; temperature range 303–393 K) (blue), precursor (**P306**; range 303–393 K) (orange), vitrimers **V306-1%** (red; range 303–503 K), **V348-5%** (purple; range 313–513 K), and **V348-9%** (green; range 313–513 K) for the high-molar-mass polymer. All master curves refer to the same reference temperature (T_{ref} = 353 K). Lines with respective slopes of 2 and 1 are used to indicate the terminal flow. Crossed circles are used to indicate characteristic frequencies (see text). Curves are vertically shifted for clarity with the shown factors.

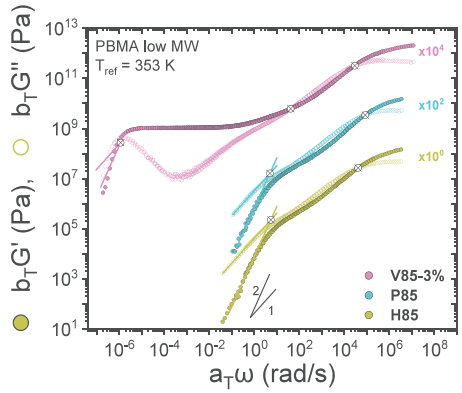

Figure 13. Master curves of the storage (G'-filled symbols) and loss (G''-open symbols) moduli of the low molar mass PBMA homopolymer (**H85**) (yellow; temperature range 303–363 K), precursor (**P85**; 303–363 K) (cyan), vitrimer **V85-3%** (magenta; 303–533 K). All master curves refer to the same reference temperature (T_{ref} = 353 K). Lines with respective slopes of 2 and 1 are used to indicate the terminal (flow) behavior. Crossed circles are used to indicate characteristic frequencies (see text). Curves are vertically shifted for clarity with the shown factors.

determine the rubber-to-glass temperature, the characteristic frequencies corresponding to the segmental process were fitted with the Vogel-Fulcher-Tammann (VFT) equation and extrapolated to a corresponding time of $\tau = 100$ *s*. A comparison with the corresponding T_g obtained from TM-DSC is shown in Figure 14. The numerical values for T_g obtained from rheology are comparable to those obtained by dielectric spectroscopy (differences between retardation and relaxation measured, respectively, by DS and rheology are small), but approximately

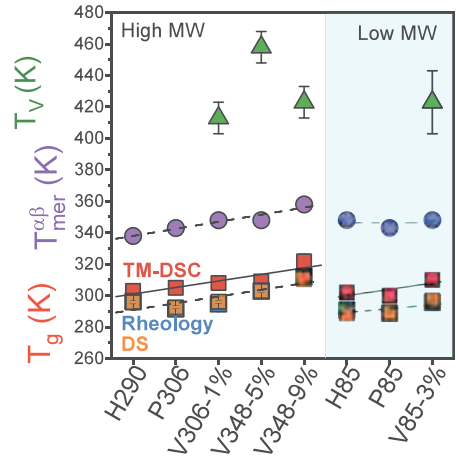

Figure 14. Rubber-to-glass temperatures T_g for the high- and low-molar-mass samples, obtained by DS (orange squares), rheology (blue squares), and TM-DSC (red squares). Additionally, T_V (green triangles) is identified as the temperature where the T-dependence of the viscoelastic shift factors changes from WLF to Arrhenius (see text). The temperature at which the α- and β-processes in DS merge to form the αβ-process is also indicated (purple circles).

10 K lower than those from TM-DSC, which is expected given the selected modulation period ($\Pi = 40$ s).

The temperature dependence of the horizontal shift factors used in the master curves of the vitrimer samples is of particular interest (the temperature dependence of the vertical shift factors, b_T, follows that of density, Figure S21). They can be used to extract the characteristic temperature, T_V, separating the segmental-dominated dynamics at lower temperatures from the bond exchange dynamics initiating flow at higher temperatures. Clearly, this definition of T_V is different from the original viscosity-based definition of the topology freezing temperature.[1] Here, T_V, defines the crossover temperature between WLF and Arrhenius shift-factor behavior. Indeed, at lower temperatures the shift factors follow the WLF equation and above, T_V, the temperature dependence follows the Arrhenius relation:

$$a_T = a_T^0 \cdot e^{\frac{E^*}{RT}} \tag{11}$$

Here, E^* is the activation energy associated with the dynamic bonds of the network. The horizontal shift factors for the vitrimer **V348-5%** are presented in Figure 15a. At lower temperatures, the WLF equation describes the shift factors well as can be deduced by the value of the χ^2 parameter ($\chi^2 < 1.5 \times 10^{-3}$). However, at higher temperatures, the WLF equation fails to describe the data ($\chi^2 \sim 3 \times 10^{-3}$). This approach can provide an approximate value for T_V as it requires specific stringent criteria in the value of the χ^2 parameter. A more sensitive approach to locate changes in the temperature dependence of the shift factors is by plotting $\left(-d(\log a_T)/d\left(\frac{1}{T}\right)\right)^{-1/2}$ vs $1/T$.[61] In this representation, an Arrhenius temperature dependence appears as a horizontal line, allowing an easier determination of T_V (as shown in Figure 15b). We re-emphasize here that this definition of T_V, is different from the original one given by Leibler.[1] In the latter,

https://doi.org/10.1021/acs.macromol.6c01360
Macromolecules 2026, 59, 10544–10556

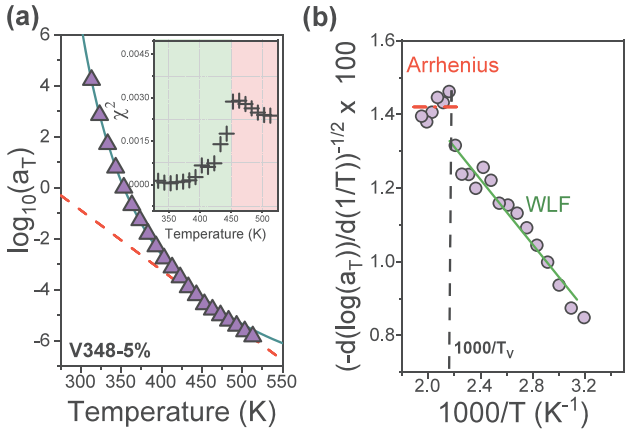

Figure 15. (a) Horizontal shift factors, a_T, used in the master curve of Figure 12 plotted against T for the vitrimer **V348-5%.** Fits to Arrhenius and WLF dependences are indicated by the red and green lines, respectively. The "transition" from WLF (green solid line) to Arrhenius (red dashed line) behavior is identified by analyzing the values of χ^2 parameter (inset). (b) Derivative analysis of the shift factors with respect to inverse temperature. The vertical black dotted line is used to determine T_V.

the transition temperature was conventionally defined as the temperature where the viscosity of the melt corresponds to 10^{12} Pa·s.

To extract the activation energy of the bond exchange dynamics we employ solely the high temperature data. From the Arrhenius temperature dependence of the shift factors (Figure S22) we extract the following activation energies: 93 ± 5, 94 ± 2, 80 ± 2 kJ/mol, for vitrimers **V306-1%**, **V348-5%**, and **V348-9%**, respectively. These activation energies are typically, 5–6 times higher than the reported activation energy (~15.9 kJ/mol) for the metathesis reaction kinetics as measured for small molecules in their bulk state. We mention here that high activation energies have been previously reported for vitrimers based on dioxaborolane bond exchange in the high-T_g polymers poly(methyl methacrylate)[13] and poly(ethyl methacrylate).[35] In addition, much lower values were reported for polybutadiene vitrimers having a lower T_g and minimal or no entanglements.[16,27] These activation energies can be compared with the respective energies for the segmental process as recently suggested.[29,31,35] The comparison of the characteristic frequencies corresponding to the terminal, f_{term} (i.e., the bond exchange) and segmental processes, f_α, is made in Figure S23, where the ratio $\frac{f_{term}}{f_\alpha}$ is plotted as a function of inverse temperature. The two processes appear to have similar activation energies when examined over the same temperature range. We need to mention, however, that this conclusion is based on a long extrapolation of the segmental process from lower temperatures (by about 100 K but with a fixed f_∞ value of 10^{13} Hz).

Another issue is related to the thermal stability of the polymer matrix (homopolymers and vitrimer precursors, Figure S15). TGA indicated an expected lower thermal stability for the lower molar mass polymers attributed to the higher concentration of chain-ends. This is the reason why we do not report apparent activation energies for the low-molar-mass vitrimer (**V85-3%**). To test the thermal stability of the remaining vitrimers we performed kinetic studies in rheology by making consecutive frequency sweeps over a period of 8 h at a temperature of 473 K. A slow evolution of the storage and loss moduli was found in the **V348-5%** (Figure S24) as compared to the stable homopolymer (**H290**) and vitrimer precursor (**P306**) samples (Figure S25). For **V348-5%** at a frequency of 10 rad/s, the loss modulus increased by a factor of two whereas the storage modulus changed by 4%. However, this slow process does not affect the activation energies extracted from the crossing of the storage and loss moduli at higher temperatures.

The different characteristic temperatures for the vitrimers ($T_g < T_{mer}^{\alpha\beta} < T_V$; $T_{mer}^{\alpha\beta}$ is the characteristic temperature corresponding to the merging of the α- and β-processes in Figure 4), can be discussed with the help of Figure 14. Cross-linking affects both local segmental dynamics (T_g) and the global dynamics associated with the network formation. Figure 14 depicts a similar dependence (increase) of T_g and of the characteristic merging temperature ($T_{mer}^{\alpha\beta}$). This is primarily due to the stiffening of the backbone by the dynamic cross-links and the insensitivity of the β-process to the dynamic cross-links. In addition, rheology provided the characteristic topology freezing temperature, T_V, associated with the change in the temperature dependence of the shift factors. For the current PBMA vitrimers the following relation appears: $\frac{T_V}{T_g} \sim 1.4–1.5$.

4. CONCLUSIONS

A series of dioxaborolane-based poly(*n*-butyl methacrylate) (PBMA) vitrimers were synthesized, and their thermal, viscoelastic and dynamic properties were investigated as a function of the molar mass of the vitrimer precursor and cross-linking density of the network. By means of thermodynamic (DSC, TM-DSC) and dynamic (rheology, TM-DSC, DS) measurements we showed that the dynamic bonds stiffen the polymer backbone, slow down the segmental process and increase T_g. Furthermore, we found that vitrimers do not influence the local processes below T_g.

The viscoelastic properties were discussed in the light of the topology freezing temperature, T_V, separating segmental-controlled dynamics at lower temperatures from the bond exchange mechanism at higher temperatures initiating flow. The derivative approach applied to the viscoelastic shift factors was found to be a practical method to locate T_V. With respect to the flow properties, an activation energy of ~ 90 kJ/mol was found for the zero-shear viscosity of the melt, similar to the segmental dynamics within the same temperature range, but much larger than the activation energy of dioxaborolane metathesis (16 kJ/mol) reported[13] for small molecules in bulk.

The first pressure investigation on vitrimers examined the pressure sensitivity of the segmental dynamics through the apparent activation volume, $\Delta V^{\#}$. It was shown that the segment in the vitrimers is modified and that dynamic bonds contribute to an effective unit of relaxation (e.g., an effective segment) ~20% larger than in the homopolymer. Our results demonstrate that the *segment* should be redefined in theories of vitrimer dynamics to include the dynamic bonds. A close examination of the dynamic ratio of the activation energies at constant volume and at constant pressure revealed that the segmental dynamics in the vitrimers is controlled by intramolecular barriers. Studies in vitrimers with a variety of chemistries and different rubber-to-glass temperatures will further elucidate the

https://doi.org/10.1021/acs.macromol.6c01360
Macromolecules 2026, 59, 10544–10556

origin of the segmental process and the associated fundamental unit of relaxation.

■ ASSOCIATED CONTENT

Supporting Information

The Supporting Information is available free of charge at https://pubs.acs.org/doi/10.1021/acs.macromol.6c01360.

Additional information on (1) materials and methods, (2) synthetic protocols, (3) thermal properties, (4) dielectric spectroscopy, (5) rheology, including (6) equilibration kinetics (PDF)

■ AUTHOR INFORMATION

Corresponding Authors

Nathan J. Van Zee – *Chimie Moléculaire, Macromoléculaire, Matériaux, ESPCI Paris, Université PSL, CNRS, Paris 75005, France;* orcid.org/0000-0002-7899-9163; Email: nathan.van-zee@espci.psl.eu

Renaud Nicolaÿ – *Chimie Moléculaire, Macromoléculaire, Matériaux, ESPCI Paris, Université PSL, CNRS, Paris 75005, France;* orcid.org/0000-0003-1165-2592; Email: renaud.nicolay@espci.psl.eu

George Floudas – *Department of Physics, University of Ioannina, Ioannina 45110, Greece; Max Planck Institute for Polymer Research, Ackermannweg 10, Mainz 55128, Germany;* orcid.org/0000-0003-4629-3817; Email: gfloudas@uoi.gr

Authors

Michail Danikas – *Department of Physics, University of Ioannina, Ioannina 45110, Greece*

Matteo Conti – *Chimie Moléculaire, Macromoléculaire, Matériaux, ESPCI Paris, Université PSL, CNRS, Paris 75005, France*

Johan Mattsson – *School of Physics and Astronomy, University of Leeds, Leeds LS2 9JT, United Kingdom;* orcid.org/0000-0001-7057-2192

Laurence Ramos – *Laboratoire Charles Coulomb (L2C),Université Montpellier, CNRS, Place Eugène bataillon – cc 069, Montpellier 34090, France;* orcid.org/0000-0003-2859-5133

Complete contact information is available at: https://pubs.acs.org/doi/10.1021/acs.macromol.6c01360

Funding

This work is part of The ReBond Project, which has received funding from the Horizon Europe Programme (Marie Skłodowska-Curie Actions) of the Marie Skłodowska-Curie Doctoral Network (HORIZON-MSCA-2022-DN-01), under ReBond REA Grant Agreement No. 101119786.

Notes

The authors declare no competing financial interest.

■ ACKNOWLEDGMENTS

M.D. and M.C. were supported by The ReBond Project, which has received funding from the Horizon Europe Programme (Marie Skłodowska-Curie Actions) of the Marie Skłodowska-Curie Doctoral Network (HORIZON-MSCA-2022-DN-01), under ReBond REA Grant Agreement No. 101119786. L.R. thanks Anne-Caroline Genix for useful discussions.

■ REFERENCES

(1) Montarnal, D.; Capelot, M.; Tournilhac, F.; Leibler, L. Silica-like Malleable Materials from Permanent Organic Networks. *Science* **2011**, *334*, 965–968.

(2) Capelot, M.; Unterlass, M. M.; Tournilhac, F.; Leibler, L. Catalytic Control of the Vitrimer Glass Transition. *ACS Macro Lett.* **2012**, *1*, 789–792.

(3) Van Zee, N. J.; Nicolaÿ, R. Vitrimers: Permanently Crosslinked Polymers with Dynamic Network Topology. *Prog. Polym. Sci.* **2020**, *104*, 101233.

(4) Denissen, W.; Winne, J. M.; Du Prez, F. E. Vitrimers: Permanent Organic Networks with Glass-like Fluidity. *Chem. Sci.* **2016**, *7*, 30–38.

(5) Luo, J.; Demchuk, Z.; Zhao, X.; Saito, T.; Tian, M.; Sokolov, A. P.; Cao, P.-F. Elastic Vitrimers: Beyond Thermoplastic and Thermoset Elastomers. *Matter* **2022**, *5*, 1391–1422.

(6) Brutman, J. P.; Delgado, P. A.; Hillmyer, M. A. Polylactide Vitrimers. *ACS Macro Lett.* **2014**, *3*, 607–610.

(7) Denissen, W.; Rivero, G.; Nicolaÿ, R.; Leibler, L.; Winne, J. M.; du Prez, F. E. Vinylogous Urethane Vitrimers. *Adv. Funct. Mater.* **2015**, *25*, 2451–2457.

(8) Yang, Y.; Pei, Z.; Li, Z.; Wei, Y.; Ji, Y. Making and Remaking Dynamic 3D Structures by Shining Light on Flat Liquid Crystalline Vitrimer Films without a Mold. *J. Am. Chem. Soc.* **2016**, *138*, 2118–2121.

(9) Pei, Z.; Yang, Y.; Chen, Q.; Wei, Y.; Ji, Y. Regional Shape Control of Strategically Assembled Multishape Memory Vitrimers. *Adv. Mater.* **2016**, *28*, 156–160.

(10) Capelot, M.; Montarnal, D.; Tournilhac, F.; Leibler, L. Metal-Catalyzed Transesterification for Healing and Assembling of Thermosets. *J. Am. Chem. Soc.* **2012**, *134*, 7664–7667.

(11) Yang, Y.; Urban, M. W. Self-healing Polymeric Materials. *Chem. Soc. Rev.* **2013**, *42* (17), 7446–7467.

(12) Zhang, Z.; Ghezawi, N.; Li, B.; Ge, S.; Zhao, S.; Saito, T.; Hun, D.; Cao, P. F. Autonomous Self-Healing Elastomers with Unprecedented Adhesion Force. *Adv. Funct. Mater.* **2021**, *31* (4),2006298.

(13) Röttger, M.; Domenech, T.; van Der Weegen, R.; Breuillac, A.; Nicolaÿ, R.; Leibler, L. High-Performance Vitrimers from Commodity Thermoplastics Through Dioxaborolane Metathesis. *Science* **2017**, *356* (6333), 62–65.

(14) Gosecki, M.; Gosecka, M. Boronic Acid Esters and Anhydrates as Dynamic Cross-Links in Vitrimers. *Polymers* **2022**, *14*, 842.

(15) Hammer, L.; Nicolaÿ, R. Interpenetrating Vitrimers Based on Dioxaborolane Metathesis and Imine-Aldehyde Exchange. *Polym. Chem.* **2025**, *16*, 4843.

(16) Breuillac, A.; Kassalias, A.; Nicolaÿ, R. Polybutadiene Vitrimers Based on Dioxaborolane Chemistry and Dual Networks with Static and Dynamic Cross-links. *Macromolecules* **2019**, *52*, 7102–7113.

(17) Caffy, F.; Nicolaÿ, R. Transformation of Polyethylene Into a Vitrimer by Nitroxide Radical Coupling of a Bis-dioxaborolane. *Polym. Chem.* **2019**, *10*, 3107.

(18) Breuillac, A.; Caffy, F.; Vialon, T.; Nicolaÿ, R. Functionalization of Polyisoprene and Polystyrene via Reactive Processing Using Azidoformate Grafting Agents, and its Application to the Synthesis of Dioxaborolane-based Polyisoprene Vitrimers. *Polym. Chem.* **2020**, *11*, 6479.

(19) Kölsch, J. C.; Berač, C. M.; Lossada, F.; Stach, O. S.; Seiffert, S.; Walther, A.; Besenius, P. Recyclable Vitrimers from Biogenic Poly(itaconate) Elastomers. *Macromolecules* **2022**, *55*, 8032–8039.

(20) Denissen, W.; Droesbeke, M.; Nicolaÿ, R.; Leibler, L.; Winne, J. M.; Du Prez, F. E. Chemical Control of the Viscoelastic Properties of Vinylogous Urethane Vitrimers *Nat. Commun.* **2017**, *8* (1), 14857.

(21) Li, L.; Chen, X.; Jin, K.; Torkelson, J. M. Vitrimers Designed both to Strongly Suppress Creep and to Recover Original Cross-link Density

after Reprocessing: Quantitative Theory and Experiments. *Macromolecules* **2018**, *51* (15), 5537–5546.
(22) Ge, S.; Tress, M.; Xing, K.; Cao, P.-F.; Saito, T.; Sokolov, A. P. Viscoelasticity in Associating Oligomers and Polymers: Experimental Test of the Bond Lifetime Renormalization Model. *Soft Matter* **2020**, *16* (2), 390–401.
(23) Samanta, S.; Kim, S.; Saito, T.; Sokolov, A. P. Polymers with Dynamic Bonds: Adaptive Functional Materials for a Sustainable Future. *J. Phys. Chem. B* **2021**, *125* (33), 9389–9401.
(24) Meng, F.; Saed, M. O.; Terentjev, E. M. Rheology of Vitrimers. *Nat. Commun.* **2022**, *13*, 5753.
(25) Ge, S.; Samanta, S.; Li, B.; Carden, G. P.; Cao, P.-F.; Sokolov, A. P. Unravelling the Mechanism of Viscoelasticity in Polymers with Phase-Separated Dynamic Bonds. *ACS Nano* **2022**, *16* (3), 4746–4755.
(26) Ge, S.; Tsao, Y.-H.; Evans, C. M. Polymer Architecture Dictates Multiple Relaxation Processes in Soft Networks with Two Orthogonal Dynamic Bonds *Nat. Commun.* **2023**, *14* (1), 7244.
(27) Ricarte, R. G.; Shanbhag, S.; Ezzeddine, D.; Barzycki, D.; Fay, K. Time–Temperature Superposition of Polybutadiene Vitrimers. *Macromolecules* **2023**, *56* (17), 6806–6817.
(28) Soman, B.; Schweizer, K. S.; Evans, C. M. Fragile Glass Formation and Non-Arrhenius Upturns in Ethylene Vitrimers Revealed by Dielectric Spectroscopy. *Macromolecules* **2023**, *56* (1), 166–176.
(29) Martins, M. L.; Zhao, X.; Demchuk, Z.; Luo, J.; Carden, G. P.; Toleutay, G.; Sokolov, A. P. Viscoelasticity of Polymers with Dynamic Covalent Bonds: Concepts and Misconceptions. *Macromolecules* **2023**, *56* (21), 8688–8696.
(30) Mei, B.; Evans, C. M.; Schweizer, K. S. Self-Consistent Theory for Structural Relaxation, Dynamic Bond Exchange Times, and the Glass Transition in Polymeric Vitrimers. *Macromolecules* **2024**, *57* (7), 3242–3257.
(31) Carden, G. P.; Martins, M. L.; Toleutay, G.; Ge, S.; Li, B.; Zhao, S.; Sokolov, A. P. Critical Role of Free Amine Groups in the Imine Bonds Exchange in Dynamic Covalent Networks. *Macromolecules* **2024**, *57*, 8621–8631.
(32) Ricarte, R. G.; Shanbhag, S. A Tutorial Review of Linear Rheology for Polymer Chemists: Basics and Best Practices for Covalent Adaptable Networks. *Polym. Chem.* **2024**, *15*, 815–846.
(33) Porath, L. E.; Ramlawi, N.; Huang, J.; Hossain, M. T.; Derkaloustian, M.; Ewoldt, R. H.; Evans, C. M. Molecular Design of Multimodal Viscoelastic Spectra Using Vitrimers. *Chem. Mater.* **2024**, *36* (4), 1966–1974.
(34) Xia, J.; Olvera de la Cruz, M. Dynamics and Structure of Unentangled Associative Polymers. *Macromolecules* **2024**, *57*, 8793–8802.
(35) Ge, S.; Evans, C. M. Influence of Segmental Dynamics on Bond Exchange in Imine Vitrimers with Different Polymer Backbones and Cross-linkers. *Macromolecules* **2025**, *58*, 4043–4058.
(36) Wang, H.; Jiang, N.; Zhang, R.; Nicolaÿ, R.; Fustin, C.-A.; van Ruymbeke, E. Linear Viscoelasticity of Model Vitrimers: Decoding the Interplay between Bond Exchange and Segmental Dynamics. *Macromolecules* **2026**, *59*, 2818–2834.
(37) Stavropoulou, V. N.; Aldecoa-Ortueta, M.; Verde-Sesto, E.; Di Lisio, V.; Lam, A.; Pomposo, J. A.; Alegría, A.; Cangialosi, D.; Barroso-Bujans, F. Vitrimeric Behavior Revealed by Fast Scanning Calorimetry in Branched Polyglycerol Networks Cross-Linked by Reversible Enamine Bonds. *Macromolecules* **2025**, *58*, 9993–10006.
(38) Klingler, A.; Reisinger, D.; Schlögl, S.; Wetzel, B.; Breuer, U.; Krüger, J.-K. Vitrimer Transition Phenomena from the Perspective of Thermal Volume Expansion and Shape (In)stability. *Macromolecules* **2024**, *57*, 4246–4253.
(39) Matsumiya, Y.; Watanabe, H.; Urakawa, O.; Inoue, T. Experimental Test for Viscoelastic Relaxation of Polyisoprene Undergoing Monofunctional Head-to-Head Association and Dissociation. *Macromolecules* **2016**, *49* (18), 7088–7095.
(40) Stukalin, E. B.; Cai, L.-H.; Kumar, N. A.; Leibler, L.; Rubinstein, M. Self-healing of Unentangled Polymer Networks with Reversible Bonds. *Macromolecules* **2013**, *46* (18), 7525–7541.
(41) Moad, G.; Solomon, D. H. In *The Chemistry of Radical Polymerization*; Elsevier: Amsterdam, **2006**.
(42) Le Neindre, M.; Magny, B.; Nicolaÿ, R. Evaluation of Thiocarbonyl and Thioester Moieties as Thiol Protecting Groups for Controlled Radical Polymerization. *Polym. Chem.* **2013**, *4* (22), 5577–5584.
(43) Kremer, F.; Schönhals, A. In *Broadband Dielectric Spectroscopy*; Springer Berlin: Heidelberg, **2002**; pp 1–729.
(44) Floudas, G.; Paluch, M.; Grzybowski, A.; Ngai, K. L. In *Molecular Dynamics of Glass-Forming Systems. Effects of Pressure*; Springer-Verlag: Berlin Heidelberg, **2011**; pp 1–174.
(45) Mpoukouvalas, K.; Floudas, G.; Williams, G. Origin of the α, β, (βα), and "Slow" Dielectric Processes in Poly(ethyl methacrylate). *Macromolecules* **2009**, *42*, 4690–4700.
(46) Deres, A.; Floudas, G. A.; Müllen, K.; van der Auweraer, M.; De Schryver, F.; Enderlein, J.; Uji-i, H.; Hofkens, J. The Origin of Heterogeneity of Polymer Dynamics near the Glass Temperature as Probed by Defocused Imaging. *Macromolecules* **2011**, *44*, 9703–9709.
(47) Ngai, K. L.; Roland, C. M. Chemical Structure and Intermolecular Cooperativity: Dielectric Relaxation Results. *Macromolecules* **1993**, *26*, 6824–6830.
(48) Kunal, K.; Robertson, C. G.; Pawlus, S.; Hahn, S. F.; Sokolov, A. P. Role of Chemical Structure in Fragility of Polymers: A Qualitative Picture. *Macromolecules* **2008**, *41*, 7232–7238.
(49) Dudowicz, J.; Freed, K. F.; Douglas, J. F. Fragility of Glass-Forming Polymer Liquids. *J. Phys. Chem. B* **2005**, *109*, 21350–21356.
(50) Saltzman, E. J.; Schweizer, K. S. Short Time Properties, Dynamic Fragility and Pressure Effects in Deeply Supercooled Polymer Melts. *J. Phys.: Condens. Matter* **2007**, *19*, 205123.
(51) Paluch, M.; Patkowski, A.; Fischer, E. W. Temperature and Pressure Scaling of the α Relaxation Process in Fragile Glass Formers: A Dynamic Light Scattering Study. *Phys. Rev. Lett.* **2000**, *85*, 2140.
(52) Floudas, G.; Gravalides, C.; Reisinger, T.; Wegner, G. Effect of Pressure on the Segmental and Chain Dynamics of Polyisoprene Molecular Weight Dependence. *J. Chem. Phys.* **1999**, *111*, 9847.
(53) Floudas, G.; Reisinger, T. Pressure Dependence of the Local and Global Dynamics of Polyisoprene. *J. Chem. Phys.* **1999**, *111*, 5201.
(54) Floudas, G.; Fytas, G.; Reisinger, T.; Wegner, G. Pressure induced Dynamic Homogeneity in an Athermal Diblock Copolymer Melt. *J. Chem. Phys.* **1999**, *111*, 9129–9132.
(55) Floudas, G.; Mpoukouvalas, K.; Papadopoulos, P. The Role of Temperature and Density on the Glass-Transition Dynamics of Glass Formers. *J. Chem. Phys.* **2006**, *124*, 74905.
(56) Andersson, S. P.; Andersson, O. Relaxation Studies of Poly(propylene glycol) under High Pressure. *Macromolecules* **1998**, *31*, 2999–3006.
(57) Williams, G. Complex Dielectric Constant of Dipolar Compounds as a Function of Temperature, Pressure and Frequency. *Faraday Soc.* **1964**, *60*, 1548.
(58) Naoki, M.; Endou, H.; Matsumoto, K. Pressure Effects on Dielectric Relaxation of Supercooled o-Terphenyl. *J. Phys. Chem.* **1987**, *91*, 4169.
(59) Zoller, P.; Walsh, D. J. In *Standard Pressure – Volume - Temperature Data for Polymers*; Technomic Publishing Company, Inc.: Lancaster, PA 17604, U.S.A, **1995**.
(60) Van Gurp, M.; Palmen, J. Time-Temperature Superposition for Polymeric Blends. *Rheol. Bull.* **1998**, *67*, 5–8.
(61) Hansen, C.; Stickel, F.; Berger, T.; Richert, R.; Fischer, E. W. Dynamics of Glass-Forming Liquids. III Comparing the Dielectric α- and β-relaxation of 1-Propanol and o-Terphenyl. *J. Chem. Phys.* **1997**, *107*, 1086–1093.

https://doi.org/10.1021/acs.macromol.6c01360
Macromolecules 2026, 59, 10544–10556